ISSN 1064-2307, Journal of Computer and Systems Sciences International, 2021, Vol. 60, No. 2, pp. 315–332. © Pleiades Publishing, Ltd., 2021.
Russian Text © The Author(s), 2021, published in Izvestiya Akademii Nauk, Teoriya i Sistemy Upravleniya, 2021, No. 2, pp. 138–155.

CONTROL SYSTEMS OF MOVING OBJECTS

Estimation of an Inertia Tensor and Automatic Balancing of a Microsatellite Mockup on an Air-Bearing Testbed

D. S. Ivanov[a,*], T. A. Ivanova[b], N. A. Ivlev[c], M. Yu. Ovchinnikov[a], and D. S. Roldugin[a]

[a] *Keldysh Institute of Applied Mathematics, Russian Academy of Sciences, Moscow, Russia*

[b] *Peoples' Friendship University of Russia, Moscow, Russia*

[c] *Moscow Institute of Physics and Technology (National Research University), Moscow, Russia*

**e-mail: danilivanovs@gmail.com*

Received May 12, 2020; revised May 18, 2020; accepted July 27, 2020

Abstract—This paper considers the problem of determining the position of the center-of-mass and inertia tensor of a microsatellite mockup on an air-bearing testbed by using optical measurements. The position of the mockup's center of mass can be shifted relative to the suspension's center by using a system of electrodynamic linear actuators and loads fixed on them. Using the equations of motion of the mockup on an aerodynamic suspension and measurements of its angular position, the inertia tensor and center-of-mass position of the model are estimated. Based on these estimates, the linear actuators move to set the desired center-of-mass position relative to the suspension point. The developed algorithm for automatic balancing of the microsatellite mockup is experimentally investigated.

DOI: 10.1134/S1064230721020088

INTRODUCTION

Presently, there are two main laboratory approaches to test motion control systems of spacecrafts in terms of their dynamics: the use of aerodynamic suspensions and the use of air-bearing tables, as well as their combination. Due to the air cushion between the surface of the table and the support of a microsatellite control system mockup, the air-bearing testbed enables the free planar translational motion and uniaxial rotation of the apparatus. These testbeds can be used for testing control algorithms of a single model, as well as for testing the motion control of a group of microsatellites [1–3].

Spherical aerodynamic suspensions are widely used for laboratory simulation of the attitude motion of microsatellites. The suspension consists of two hemispheres nested in one another. The outer hemisphere has a certain (generally small) number of air holes. This makes it possible to create an air gap between the outer and inner spheres, which almost eliminates friction. The suspension has three degrees of freedom; however, generally, it can indefinitely rotate only about the vertical axis because the platform that represents the microsatellite or its attitude control system is installed on the inner sphere [4, 5].

One of the first testbeds was created at the Army Ballistic Missile Agency (United States) in 1959 [6]. The complex construction of the pedestal and platform that hosted the elements of the satellite's onboard systems enabled a roll angle of up to 120°. The first problem investigated using aerodynamic suspensions was investigating the effect of energy dissipation (fuel in tanks, nutation dampers, and flywheels) on a satellite's motion. Currently, large space companies and agencies have at their disposal testbeds designed to simulate the motion of mockups that include most satellite onboard systems [7, 8].

The first small (load-carrying capacity up to 100 kg) testbed with a spherical suspension was created at Stanford in 1975 [9]. Presently, small testbeds are common in European and American universities. For instance, a platform on an aerodynamic suspension available at the National Institute of Statistics and Geography (Mexico) has a mass of only 35 kg. The platform is equipped with accelerometers, gyroscopes, magnetometer, solar sensor, magnetic coils, flywheels, and balancing system [10]. Its roll angle is limited to 50°.

An advantage of a small mockup on a suspension is that it can be placed in a Helmholtz cage. The cage provides an adjustable magnetic field to simulate the orbital motion of a satellite. This is in good agreement with the size and capabilities of small satellites: they often have magnetic coils as their main control elements. Thus, experiments in a simulated magnetic field become both important and feasible because Helmholtz coils have a small region of uniformity. Such testbeds are available, for instance, at the Univer-

sity of Strathclyde in Glasgow [11], University of Naples Federico II [12], Massachusetts Institute of Technology [13], and University of Brasília [14]. These testbeds make it possible to install only specially designed mockups of attitude control systems (rather than the entire satellites) on suspensions.

An advantage of a spherical aerodynamic suspension is the straightforward interpretation of experimental results in terms of outer space flight. The motion of both the bodies (the satellite and the mockup on a suspension) is described by the same equations, the only difference being in the external disturbances and incomplete freedom of rotation of the mockup through one or two angles. The main source of the disturbances acting on the mockup is the gravitational torque, which is due to the displacement of its center of mass relative to its center of rotation. In this case, even though the torque dominates, it can be reduced using a balancing system of movable loads installed on the control system mockup. For correct operation of the balancing system, the position of the center of mass of the model needs to be estimated. If the center of mass is below the center of rotation, then the mockup moves like a mathematical pendulum. The models in which the center of pressure is above the center of mass are preferable: these mockups do not tilt to either side but oscillate with small amplitude. The balancing can be carried out by manually shifting the movable loads upon evaluating the period of oscillations of the mockup [15]. However, this approach is based on trial and error and takes a long time to set the center of mass at an acceptable distance from the center of pressure. In contrast, when the loads on the mockup are moved using linear electromechanical actuators, the automatic balancing system significantly reduces the balancing time and increases the balancing accuracy. However, the automatic balancing requires estimating the position of the center of mass. This estimation can be carried out using onboard algorithms for processing sensor measurements, as well as using an external attitude determination system [16–18].

To fine-tune the algorithms that control the attitude motion of the mockup on an aerodynamic suspension, in addition to reducing the value of the gravitational torque by balancing, it is also required to estimate the inertia tensor of the model. The inertia tensor is generally computed using special software while specifying the position and mass of all model components. However, the distribution of masses within each block of the model is known approximately, which is why the inertia tensor is estimated with quite a large error. The inertia tensor can be determined by attitude measurements while controlling the motion of the mockup on an aerodynamic suspension, as was done in [19–21]. In those works, however, the magnitude of the control action was assumed to be known and both the inertia tensor and position of the center of mass of the mockup were determined using algorithms based on the least squares or dynamic filtering. Unfortunately, control system designers do not always have calibrated actuators (e.g., flywheels or magnetic coils) at their disposal. Thus, in contrast to the previous publications, in this paper, we estimate the inertia tensor and position of the center of mass of the model based only on the information about the displacement of the balancing loads. Two stages of the balancing procedure are considered. At the first stage, by measuring the angular position of the mockup and by moving the loads, the inertia tensor is estimated in the body-fixed frame of reference with the origin at the suspension point, and the position of the mockup's center of mass is estimated with respect to the suspension point. At the second stage, assuming that the inertia tensor is known, the position of the center of mass is estimated in real time and the iterative procedure for shifting this center to the desired position by using the system of movable loads is executed.

1. TESTBED FOR SIMULATING THE ATTITUDE MOTION OF MICROSATELLITES

In this study, we employ a testbed for testing attitude control algorithms of microsatellites that was developed by Sputnix [22]. The testbed includes a magnetic field simulator, sun simulator, mockup of a microsatellite attitude control system, and aerodynamic suspension (see Fig. 1). Due to the air cushion, this mockup is capable of three-axis attitude motion with respect to the suspension point.

Due to imperfect balancing, the position of the suspension point does not coincide with the mockup's center of mass, thus giving rise to the gravitational torque, which affects its motion. To reduce the effect of the gravitational torque, the mockup has a two-level balancing system: the direct manual positioning of its center of mass relative to the center of the suspension by using the loads moved along the axes of the body-fixed frame of reference and the software-controlled balancing system. This balancing system consists of six linear actuators, with two actuators along each axis of the body-fixed frame (see Fig. 2). The linear actuator is capable of moving the load in the range of [–5; 5] cm with an accuracy of 1 mm. The weight of the load together with the moving part of the linear actuator is 15.6 g.

To determine the attitude motion of the mockup, we use a system of optical measurements, which is based on processing images from the camera fixed on the geomagnetic field simulator. On the image, the

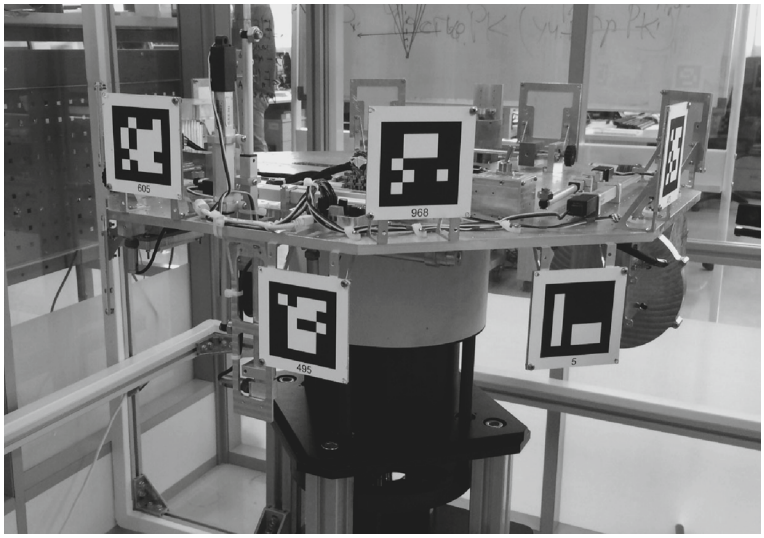

Fig. 1. Mockup of attitude control system on an aerodynamic suspension.

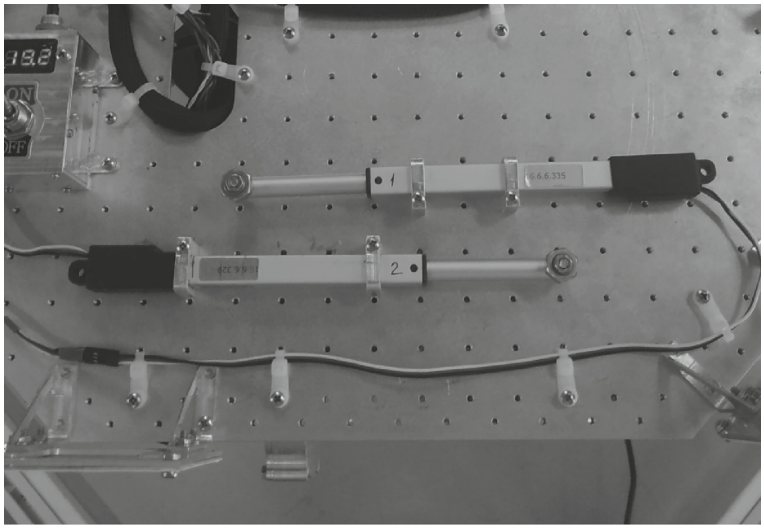

Fig. 2. Linear electromechanical actuators as part of the balancing system.

special labels made on the mockup are recognized (see Fig. 3) and its angular position relative to the stationary laboratory frame of reference is determined. The origin of the laboratory frame is at the center of the suspension; the z-axis is directed to the zenith, while the x- and y-axes are perpendicular to one another and are in the plane of the local horizon. The accuracy of determining the angular position of the mockup by using the optical measurement system is $\sigma_{meas} = 0.2°$ with the frequency of incoming measurements being approximately 5 Hz.

In this paper, we estimate the inertia tensor of the mockup in the body-fixed frame of reference with the origin at its center of mass and evaluate the vector that describes the position of the center of mass relative to the suspension point, by processing the independent optical measurements when the mockup on an aerodynamic suspension is in passive motion. This problem is solved using the linear actuators that move the balancing loads. The attitude measurements made during the experiments are used for postexperimental processing. Using the least squares method, we determine the inertia tensor and position of the center of mass that minimize the squared difference between the predicted and experimental measurements of the mockup's angular position.

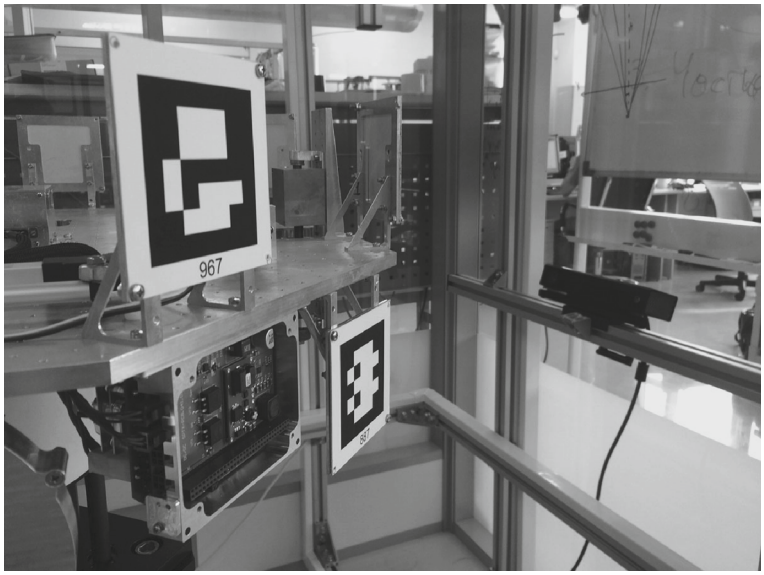

Fig. 3. Labels for determining the attitude motion of the mockup and the camera fixed on the magnetic field simulator.

Below we present the main approximate dynamic characteristics of the attitude control system mockup. Using SolidWorks, we computed the preliminary components of the inertia tensor without taking into account the mockup's cabling. In the frame of reference with the origin at the center of mass, these components have the following values:

$$\hat{\mathbf{J}} = \begin{bmatrix} 0.3309 & 0.0018 & 0.0373 \\ 0.0018 & 0.5253 & 0.0012 \\ 0.0373 & 0.0012 & 0.8120 \end{bmatrix} \text{kg m}^2.$$

The total mass of the mockup is $m = 14.24$ kg.

2. EQUATIONS OF MOTION FOR THE MOCKUP ON AN AERODYNAMIC SUSPENSION

The motion of the mockup is described by dynamic Euler equations. The variables used can be divided into two groups. The first group includes the components ω_1, ω_2, and ω_3 of the absolute angular velocity $\boldsymbol{\omega}$ of the microsatellite in the body-fixed frame of reference. For attitude description, we use quaternion $(\mathbf{q}, q_0)$, where $\mathbf{q}$ and q_0 are its vector and scalar components, respectively [23]. Euler's dynamic equations of motion of a rigid body relative to a fixed point have the form

$$\mathbf{J}\frac{d\boldsymbol{\omega}}{dt} + \boldsymbol{\omega} \times \mathbf{J}\boldsymbol{\omega} = \mathbf{M}, \tag{2.1}$$

where mechanical torque $\mathbf{M}$ includes both control $\mathbf{M}_{\text{cont}}$ and disturbing torques, i.e., $\mathbf{M} = \mathbf{M}_{\text{cont}} + \mathbf{M}_{\text{dist}}$. For the microsatellite, $\mathbf{J}$ is the inertia tensor computed in the body-fixed frame of reference with the origin at the center of mass. In this case, its axes are usually directed along the principal axes of the microsatellite. In the case of the mockup, there are two variants. We can fix the body-fixed frame at the mockup's center of mass. In this case, the equations are the same, and $\mathbf{J}$ is the inertia tensor in the principal central axes. However, this approach forces us to take into account additional disturbances and the motion of the center of mass relative to the center of rotation. That is why the following more reasonable approach is generally employed: describing the motion of the mockup relative to its center of rotation. This makes the form of tensor $\mathbf{J}$ more complex but simplifies the form of the disturbances acting on the microsatellite. Inertia tensor $\mathbf{J}$ can be represented as follows:

$$\mathbf{J} = \begin{pmatrix} I_{11} + mr_2^2 + mr_3^2 & I_{12} - mr_1r_2 & I_{13} - mr_1r_3 \\ I_{12} - mr_1r_2 & I_{22} + mr_1^2 + mr_3^2 & I_{23} - mr_2r_3 \\ I_{13} - mr_1r_3 & I_{23} - mr_2r_3 & I_{33} + mr_1^2 + mr_2^2 \end{pmatrix}, \tag{2.2}$$

where I_{ij} are the components of tensor inertia $\mathbf{I}$ for the mockup's center of mass and $\mathbf{r}$ is the vector that connects its center of rotation with its center of mass. We assume that $\mathbf{I}$ is the inertia tensor of the entire model, including the movable loads, which are initially fixed. The relationship between the inertia tensors with the loads and without them is written as follows:

$$\mathbf{I} = \hat{\mathbf{I}} - \sum_{i=1}^{N} m_i(\mathbf{r}_i^2 - \mathbf{r}_i\mathbf{r}_i^{\mathrm{T}}),$$

where $\hat{\mathbf{I}}$ is the initial inertia tensor of the mockup without the balancing loads, $\mathbf{r}_i$ is the position of the ith load in the body-fixed frame, m_i is its mass, and N is the number of loads. When the loads are moved by vector $d\mathbf{r}_i$, new inertia tensor $\tilde{\mathbf{I}}$ has the form

$$\tilde{\mathbf{I}} = \hat{\mathbf{I}} - \sum_{i=1}^{N} m_i((\mathbf{r}_i + d\mathbf{r}_i)^2 - (\mathbf{r}_i + d\mathbf{r}_i)(\mathbf{r}_i + d\mathbf{r}_i)^{\mathrm{T}}).$$

Then, the variation in the inertia tensor when moving the loads is computed by the following formula:

$$\Delta\mathbf{I} = \tilde{\mathbf{I}} - \hat{\mathbf{I}} = \sum_{i=1}^{N} m_i(d\mathbf{r}_i^2 + 2(\mathbf{r}_i, d\mathbf{r}_i)^2 - \mathbf{r}_i d\mathbf{r}_i^{\mathrm{T}} - d\mathbf{r}_i\mathbf{r}_i^{\mathrm{T}} - d\mathbf{r}_i d\mathbf{r}_i^{\mathrm{T}}). \tag{2.3}$$

Dynamic equations (2.1) are supplemented with the kinematic equations that, when using quaternion $(\mathbf{q}, q_0)$ to describe the angular position, have the following form:

$$\begin{pmatrix} \dfrac{d\mathbf{q}}{dt} \\ \dfrac{dq_0}{dt} \end{pmatrix} = \frac{1}{2}\begin{pmatrix} 0 & \omega_3 & -\omega_2 & \omega_1 \\ -\omega_3 & 0 & \omega_1 & \omega_2 \\ \omega_2 & -\omega_1 & 0 & \omega_3 \\ -\omega_1 & -\omega_2 & -\omega_3 & 0 \end{pmatrix}\begin{pmatrix} \mathbf{q} \\ q_0 \end{pmatrix}. \tag{2.4}$$

Let us regard the gravitational torque as a disturbing torque, which is written in the body-fixed frame of reference at the suspension point as follows:

$$\mathbf{M}_{ep} = mg\mathbf{r} \times \mathbf{A}\begin{bmatrix} 0 & 0 & -1 \end{bmatrix}^{\mathrm{T}}, \tag{2.5}$$

where $\mathbf{A}$ is a direction cosine matrix that specifies the transition from the laboratory frame of reference to the body-fixed frame, m is the total mass of the mockup, and g is gravitational acceleration.

Let us investigate the variation in radius vector $\mathbf{r}$, which describes the position of the center of mass and is defined in the frame of reference with the origin at the suspension point, when moving the loads by vectors $d\mathbf{r}_i$. Before moving the loads, the vector is computed as follows:

$$\mathbf{r} = \frac{\hat{m}\hat{\mathbf{r}} + \sum_{i=1}^{N} m_i\mathbf{r}_i}{m},$$

where $\hat{\mathbf{r}}$ is the radius vector to the center of mass for the mockup without the loads and $\hat{m}$ is the mass of the mockup without the loads. Once the loads are moved by $d\mathbf{r}_i$, the position of the center of mass $(\tilde{\mathbf{r}})$ is determined by the following expression:

$$\tilde{\mathbf{r}} = \frac{\hat{m}\hat{\mathbf{r}} + \sum_{i=1}^{N} m_i(\mathbf{r}_i + d\mathbf{r}_i)}{m}.$$

Then, the displacement of the center of mass is found from the following expression:

$$d\mathbf{r} = \frac{\sum_{i=1}^{N} m_i d\mathbf{r}_i}{m}. \tag{2.6}$$

3. TECHNIQUE FOR ESTIMATING THE INERTIA TENSOR AND CENTER OF MASS OF THE MOCKUP ON AN AERODYNAMIC SUSPENSION BY USING THE BALANCING SYSTEM

To carry out the laboratory investigation of the attitude determination and control algorithms, it is necessary that the motion of the mockup on an aerodynamic suspension be as similar to its orbital motion as possible. However, the difficulty is that the mockup's center of mass shifts from the suspension point, which gives rise to the gravitational torque. To reduce its effect on the motion of the mockup by using the balancing loads, the position of its center of mass must be set in the neighborhood of the suspension point as accurately as possible. To accurately compute the displacement of the loads, it is required to estimate the position of the center of mass based on the measurements provided by the attitude determination system. In addition, it is required to develop a technique for estimating the inertia tensor (together with the estimation of the center-of-mass position) because it also directly affects the motion of the system and it is known only approximately from the preliminary computations.

Let us consider the free motion of the mockup on an aerodynamic suspension (i.e., the case where the mockup is not affected by the control torque from the flywheels or magnetic coils). Its motion is completely determined by gravitational torque (2.5). Suppose that the balancing loads are initially in the zero position. The motion of the model is determined by equations (2.1) and (2.4). During free motion, the attitude determination system accumulates its measurement data, i.e., the quaternion components measured at a certain frequency. Then, at a known instant, the loads are moved by known value $d\mathbf{r}_i$, thereby changing the position of the center of mass relative to the suspension point in accordance with formula (2.6) and inertia tensor in accordance with formula (2.3). Once the loads are shifted, the mockup continues its free motion and the measurements of its angular position are accumulated.

Thus, the motion of the mockup is determined by the following unknown parameters: the position of its center of mass before the displacement of the loads ($\mathbf{r}$), inertia tensor in the frame of reference fixed to the center of mass before the displacement of the loads ($\mathbf{I}$), and vector of the initial angular velocity of the mockup in the body-fixed frame of reference ($\boldsymbol{\omega}_0$). The quaternion at the initial instant Λ_0 is taken as the first measurement of the attitude determination system. Let us introduce the vector of parameters ξ to be estimated:

$$\xi = [\mathbf{r}^T, I_{11}, I_{22}, I_{33}, I_{12}, I_{13}, I_{23}, \boldsymbol{\omega}_0^{\mathrm{T}}]^{\mathrm{T}}.$$

The vector ξ completely describes the free attitude motion of the mockup on an aerodynamic suspension. By integrating the equations of motion, we can predict the angular position of the model $\hat{\Lambda}_k$ at each instant t_k. Let us construct a formula

$$\Phi(\xi) = \sum_{k=1}^{K} (\hat{\Lambda}_k - \Lambda_k)^2, \tag{3.1}$$

where Λ_k is the attitude quaternion found using the system of independent measurements.

The problem of estimating the inertia tensor and position of the center of mass is reduced to the problem of minimizing function (3.1), which is carried out numerically.

It should be noted that, due to temperature deformations of the mockup, the position of its center of mass can vary with time. Therefore, it is reasonable to estimate this position and carry out the real-time balancing of the mockup directly when testing the attitude control algorithms.

4. ESTIMATING THE INERTIA TENSOR AND POSITION OF THE CENTER OF MASS ON AN AERODYNAMIC SUSPENSION

We carried out a series of experiments based on the technique described above. Every two minutes, the loads were moved by a known value. Figure 4 shows the quaternion components found using the attitude determination system: the circles indicate the instances when the loads were displaced with displacement vector $d\mathbf{r}$ being written in square brackets.

As an example, we consider a segment of measurements in the neighborhood of the third displacement of the loads (see Fig. 5).

Let us set the initial value for the vector of parameters to be determined: the position of the mockup's center of mass is $\mathbf{r}_0 = [0\ 0\ -10^{-4}]^{\mathrm{T}}$ m, inertia tensor (which is set in accordance with the computations

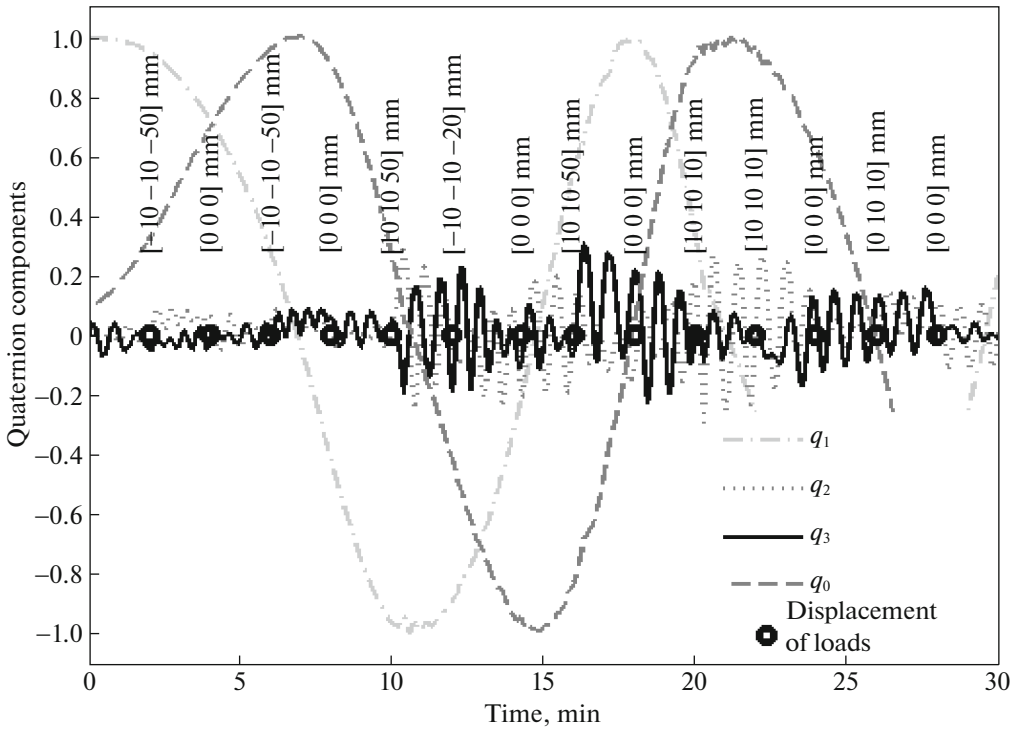

Fig. 4. Attitude measurements during the experiments.

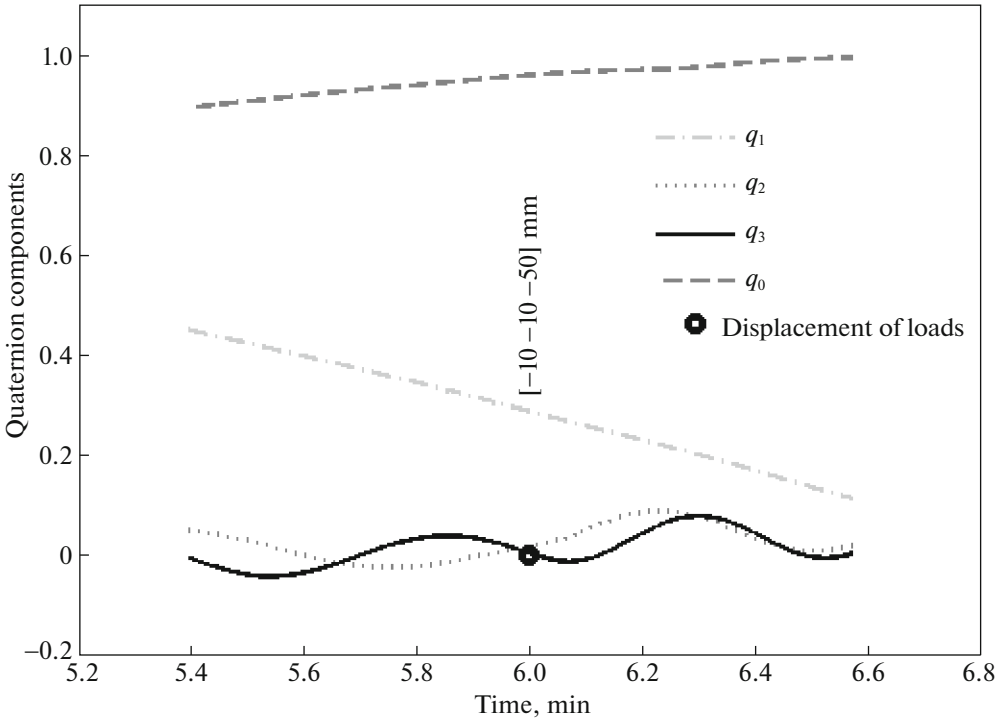

Fig. 5. Segment of measurements.

carried out using SolidWorks) is $\mathbf{I}_0 = \hat{\mathbf{I}}$, and angular velocity vector $\boldsymbol{\omega}_0$ is estimated by differentiating the direction cosine matrix with respect to the first two attitude measurements. Figure 6a compares the quaternion components found using the attitude determination system and those obtained by integrating the

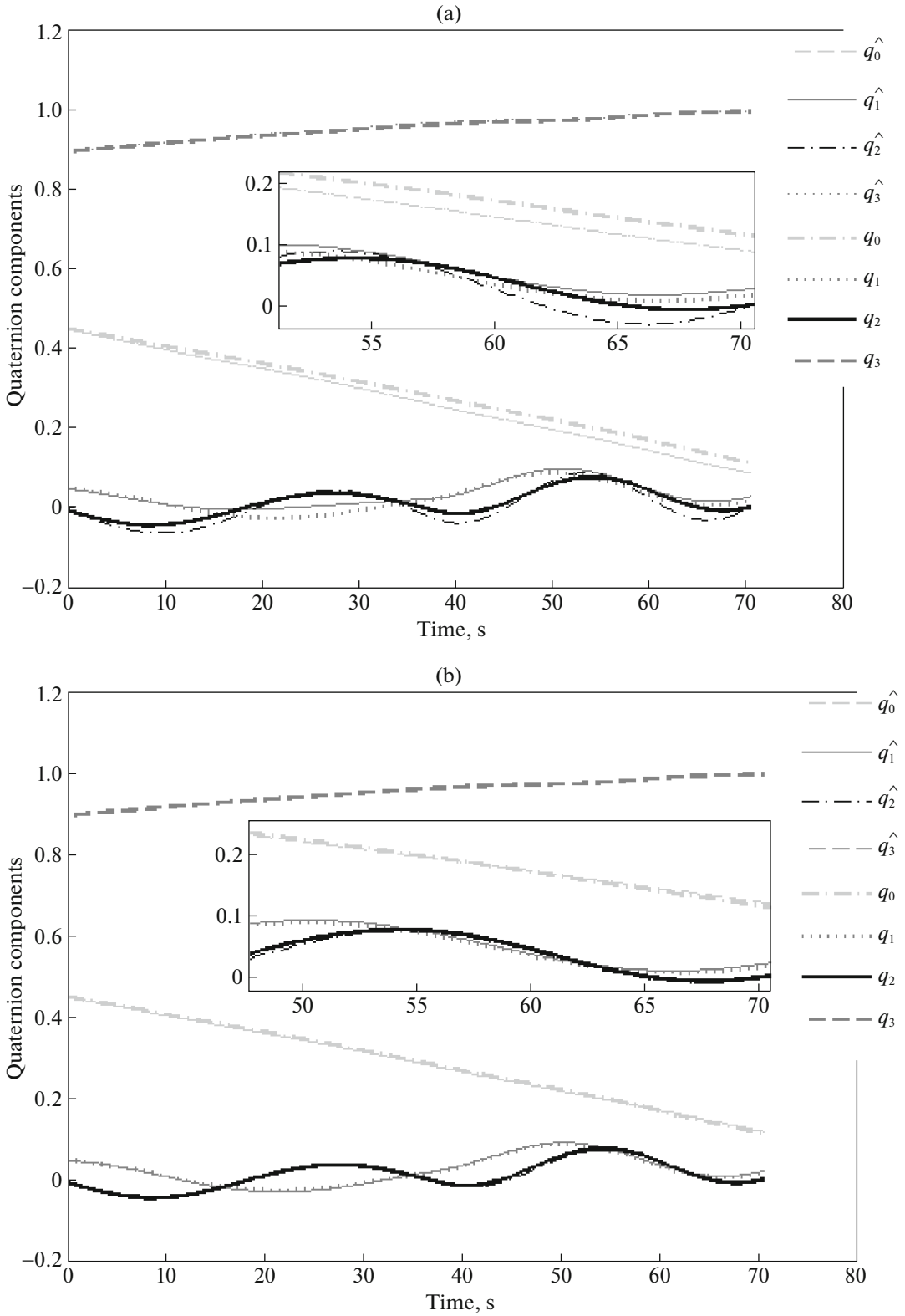

Fig. 6. Comparison between the measured and integrated angular positions (a) before and (b) after estimating $\boldsymbol{\xi}$.

equations of motion. It can be seen that the estimates of the quaternion components significantly deviate from the measured values, which can be due to the inaccurate value of the initial approximation of the vector of the estimated parameters $\boldsymbol{\xi}_0 = [\mathbf{r}_0; \mathrm{I}_0; \boldsymbol{\omega}_0]^{\mathrm{T}}$.

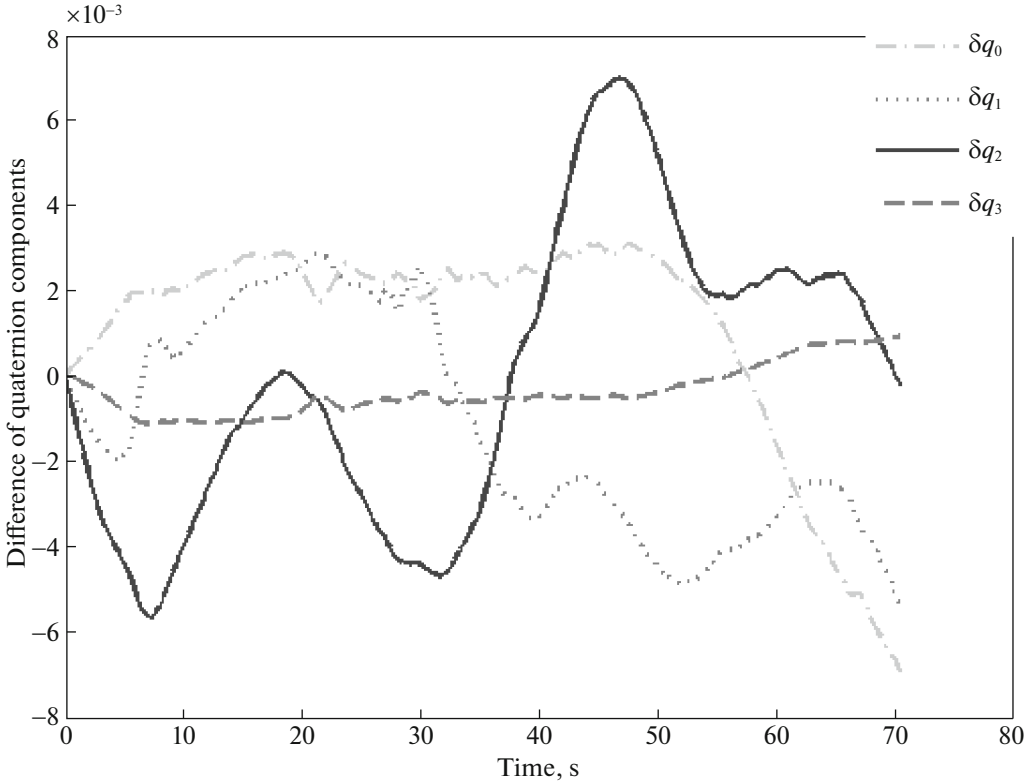

Fig. 7. Difference of quaternion components.

Let us run the iterative procedure to find vector $\boldsymbol{\xi}$ that minimizes functional (3.1). To minimize the function, we employ the Levenberg–Marquardt algorithm. As a result, we obtain the following parameters:

$$\mathbf{r}_0 = \begin{bmatrix} -9.2\times10^{-7} \\ -1.0\times10^{-7} \\ -7.9\times10^{-5} \end{bmatrix} \text{m};$$

$$\hat{\mathbf{I}} = \begin{bmatrix} 0.3565 & -0.0078 & 0.0314 \\ -0.0078 & 0.5301 & 0.0113 \\ 0.0314 & 0.0113 & 0.8782 \end{bmatrix} \text{kg m}^2;$$

$$\boldsymbol{\omega}_0 = \begin{bmatrix} -0.010 \\ -0.004 \\ 0.011 \end{bmatrix} \text{rad/s}.$$

The inertia tensor slightly differs from the one computed using SolidWorks. Figure 6b compares the measured attitude quaternion and the one obtained by integration based on the estimated parameters. Visually, these graphs coincide; however, in Fig. 7, we can see the component-wise difference that does not exceed 7×10^{-3}, which corresponds to an angular position error of 0.8°. Figure 8 shows the components of the angular velocity vector. The break in the curves at approximately 37 s is due to the displacement of the loads.

Figure 9a shows a box plot that describes the position of the center of mass in 20 experiments; based on this box plot, we can conclude that the spread for the vertical component is approximately 10^{-5} m and that for the horizontal components is approximately 5×10^{-6} m. Figure 9b shows a box plot for the components of the inertia tensor, from which it can be concluded that the spread in determining the diagonal

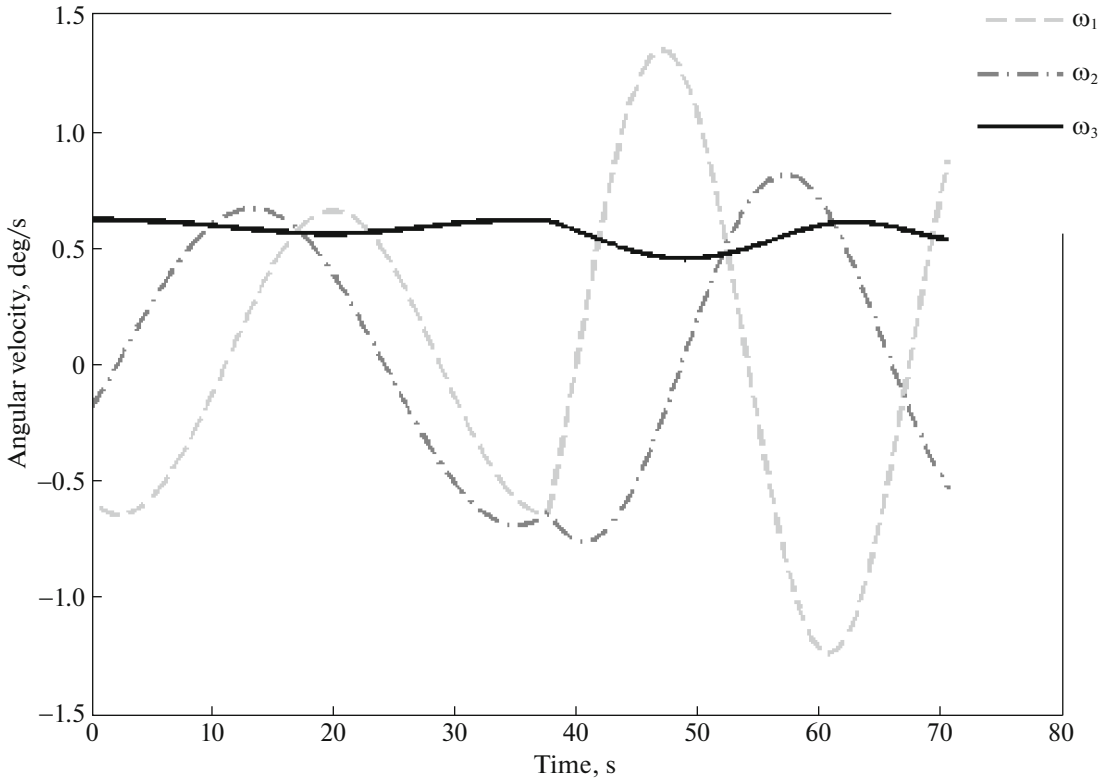

Fig. 8. Components of the angular velocity vector.

elements of the inertia tensor is approximately 0.1 kg m^2. For the estimates of the off-diagonal elements, the spread is approximately 0.05 kg m^2. Figure 9b also shows the components of the inertia tensor computed using SolidWorks. The computed values of the axial moments of inertia along the third and second axes differ noticeably from the experimental mean, which can indicate errors in the computation of the mass distribution in the components of the mockup.

5. AUTOMATIC BALANCING IN REAL TIME

To estimate the position of the center of mass in real time based on the attitude measurements, we use an algorithm based on an extended Kalman filter [24, 25]. At this stage, we assume that the estimate of the inertia tensor is known as a result of applying the least squares-based algorithm considered in Section 3. In addition, the inertia tensor remains almost constant, while the position of the center of mass can change significantly due to the thermal deformations of the mockup's platform during the experiments under the action of the heat produced by the solar simulator. This can significantly increase disturbances caused by the gravitational torque.

In the case where the position of the center of mass is determined in real time, we use the state vector of the mockup that includes the vector component of the attitude quaternion, angular velocity vector, and position of the center of mass relative to the suspension point:

$$\mathbf{x} = \begin{bmatrix} \mathbf{q} \\ \boldsymbol{\omega} \\ \mathbf{r} \end{bmatrix}.$$

The discrete model of variations in the state vector is written as follows:

$$\mathbf{x}_{k+1} = \boldsymbol{\Phi}_k \mathbf{x}_k + \mathbf{w}_k, \quad \boldsymbol{\Phi}_k = e^{\mathbf{F}_k \Delta t} \approx \mathbf{E}_{9\times 9} + \mathbf{F}_k \Delta t, \quad \mathbf{F}_k = \begin{pmatrix} -\mathbf{W}_{\boldsymbol{\omega}_k} & \frac{1}{2}\mathbf{E}_{3\times 3} & 0_{3\times 3} \\ \mathbf{J}^{-1}\mathbf{W}_{\mathbf{r}_k}\mathbf{W}_{m\mathbf{g}} & \mathbf{J}^{-1}\mathbf{F}^k_{\text{gyro}} & -\mathbf{J}^{-1}\mathbf{W}_{m\mathbf{g}} \\ 0_{3\times 3} & 0_{3\times 3} & 0_{3\times 3} \end{pmatrix}, \tag{5.1}$$

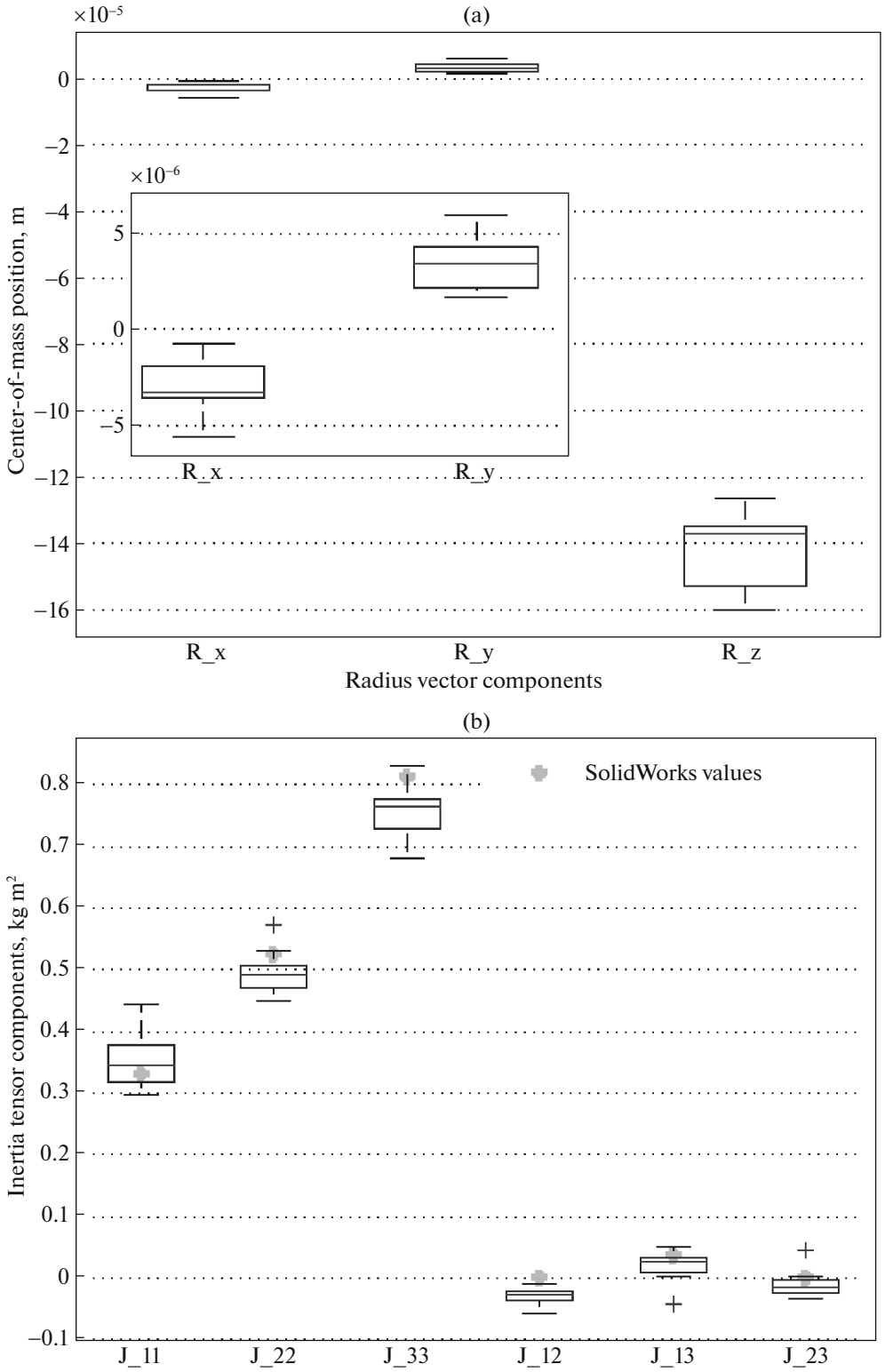

Fig. 9. Box plots for (a) position of the center of mass and (b) components of the inertia tensor in 20 experiments.

where $\mathbf{x}_k = \mathbf{x}(t_k)$, t_k is a clock instant, $\Delta t = t_{k+1} - t_k$, k is the number of a clock period of the motion determination algorithm, $0_{3\times3}$ is a 3×3 zero matrix, $\mathbf{E}_{n\times n}$ is an $n \times n$ identity matrix, $\mathbf{w}_k$ is the normally distributed discrete white error of the motion model with $\mathrm{M}(\mathbf{w}_k) = 0$ and $\mathrm{M}(\mathbf{w}_k \mathbf{w}_i^{\mathrm{T}}) = Q\delta_{ki}$, δ_{ki} is the Kronecker

symbol, $\mathbf{F}_k$ is a dynamics matrix obtained by linearization of equations of motion (2.1) and (2.4), $\mathbf{W}_\mathbf{y}$ is a skew-symmetric matrix with the elements defined by vector $\mathbf{y}$, and $\mathbf{F}^k_{\text{gyro}} = 2(\mathbf{W}_{\mathbf{J}\boldsymbol{\omega}_k}\mathbf{W}_{\boldsymbol{\omega}_k} - \mathbf{W}_{\boldsymbol{\omega}_k}\mathbf{J}\mathbf{W}_{\boldsymbol{\omega}_k})$ is a gyroscopic torque matrix.

In (5.1), we use the following discrete model of variations in the radius vector of the center of mass in the body-fixed frame of reference with the origin at the suspension point:

$$\mathbf{r}_k = \mathbf{r}_{k-1} + \mathbf{w}^r_k,$$

where $\mathbf{r}_k = \mathbf{r}(t_k)$ and $\mathbf{w}_\mathbf{r}$ is a normally distributed discrete white random variable with $\mathrm{M}(\mathbf{w}^{\mathrm{T}}_k) = 0$ and $\mathrm{M}(\mathbf{w}^r_k\mathbf{w}^{r\mathrm{T}}_i) = \mathbf{Q}^r\delta_{ki}$. Random nature of the variations in the position of the center of mass can be due to the effect of the thermal variations in the volume of the materials of the mockup, which is not taken into account in the model.

Vector component of quaternion $\mathbf{z} = \mathbf{q}$ is regarded as a measurement vector. Then, the discrete measurement model has the following form:

$$\mathbf{z}_k = \mathbf{H}\mathbf{x}_k + \boldsymbol{\psi}_k,$$

where $\mathbf{H} = \begin{bmatrix}\mathbf{E}_{3\times3} & 0_{3\times3} & 0_{3\times3}\end{bmatrix}$ and $\boldsymbol{\psi}_k$ is a normally distributed $\mathbf{w}_k$-independent white measurement error with zero expectation $\mathrm{M}(\boldsymbol{\psi}_k) = 0$ and covariance matrix $\mathrm{M}(\boldsymbol{\psi}_k\boldsymbol{\psi}^{\mathrm{T}}_i) = \mathbf{R}\delta_{ki}$.

The extended Kalman filter operates in two stages: predicting the state vector before receiving a measurement and refining the prediction when processing the measurement results. At the prediction stage, the prior estimate of the state vector $\hat{\mathbf{x}}^-_{k+1}$ is computed using the continuous equations of motion with the initial conditions given by the posterior estimate of the state vector at the previous step $\hat{\mathbf{x}}^+_k$:

$$\hat{\mathbf{x}}^-_k = \int\limits_{t_{k-1}}^{t_k} \mathbf{f}(\hat{\mathbf{x}}^+_{k-1}, t)dt,$$

where $\mathbf{f}(\mathbf{x},t)$ is the function of the right-hand sides, which can be derived from equations (2.1) and (2.4). In addition, at the prediction stage, the covariance error matrix of the state vector $\mathbf{P}_k = \mathrm{M}(\Delta\mathbf{x}_k\Delta\mathbf{x}^{\mathrm{T}}_k)$ is found, where $\Delta\mathbf{x}_k = \hat{\mathbf{x}}_k - \mathbf{x}_k$ is the estimation error of the Kalman filter. The prior matrix $\mathbf{P}^-_{k+1}$ is computed using the following discrete equation:

$$\mathbf{P}^-_{k+1} = \boldsymbol{\Phi}_k\mathbf{P}^+_k\boldsymbol{\Phi}^{\mathrm{T}}_k + \mathbf{Q}.$$

At the refinement stage, the posterior estimate of the state vector $\hat{\mathbf{x}}^+_{k+1}$ and posterior co-variation matrix $\mathbf{P}^+_{k+1}$ are computed by the formulas

$$\hat{\mathbf{x}}^+_{k+1} = \hat{\mathbf{x}}^-_{k+1} + \mathbf{K}_{k+1}(\mathbf{z}_{k+1} - \mathbf{H}\hat{\mathbf{x}}^-_{k+1}),$$

$$\mathbf{P}^+_{k+1} = (\mathbf{E}_{9\text{x}9} - \mathbf{K}_{k+1}\mathbf{H})\mathbf{P}^-_{k+1},$$

where

$$\mathbf{K}_{k+1} = \mathbf{P}^-_{k+1}\mathbf{H}^{\mathrm{T}}(\mathbf{H}\mathbf{P}^-_{k+1}\mathbf{H}^{\mathrm{T}} + \mathbf{R})^{-1}.$$

For the discrete Kalman filter, at the initial instant, it is required to specify the state vector $\mathbf{x}_0$, as well as the covariance matrices of motion model errors $\mathbf{Q}$, measurement errors $\mathbf{R}$, and initial state vector errors $\mathbf{P}_0$. Matrix $\mathbf{Q}$ can be estimated experimentally based on the values of the disturbances not taken into account in the motion model. Covariance matrix $\mathbf{R}$ is generally set as a diagonal matrix, where the variances of the measurement errors are positioned along the diagonal and are determined experimentally, i.e., $\mathbf{R} = \mathrm{diag}(\sigma^2_{\text{meas}}, \sigma^2_{\text{meas}}, \sigma^2_{\text{meas}})$. Matrix $\mathbf{P}_0$ is set taking into account the initial lack of information about state vector $\mathbf{x}_0$.

Let us consider a segment of measurements where the loads are fixed (see Fig. 10). We take measurements and, at each step, estimate the position of the center of mass. The estimated angular velocity of the

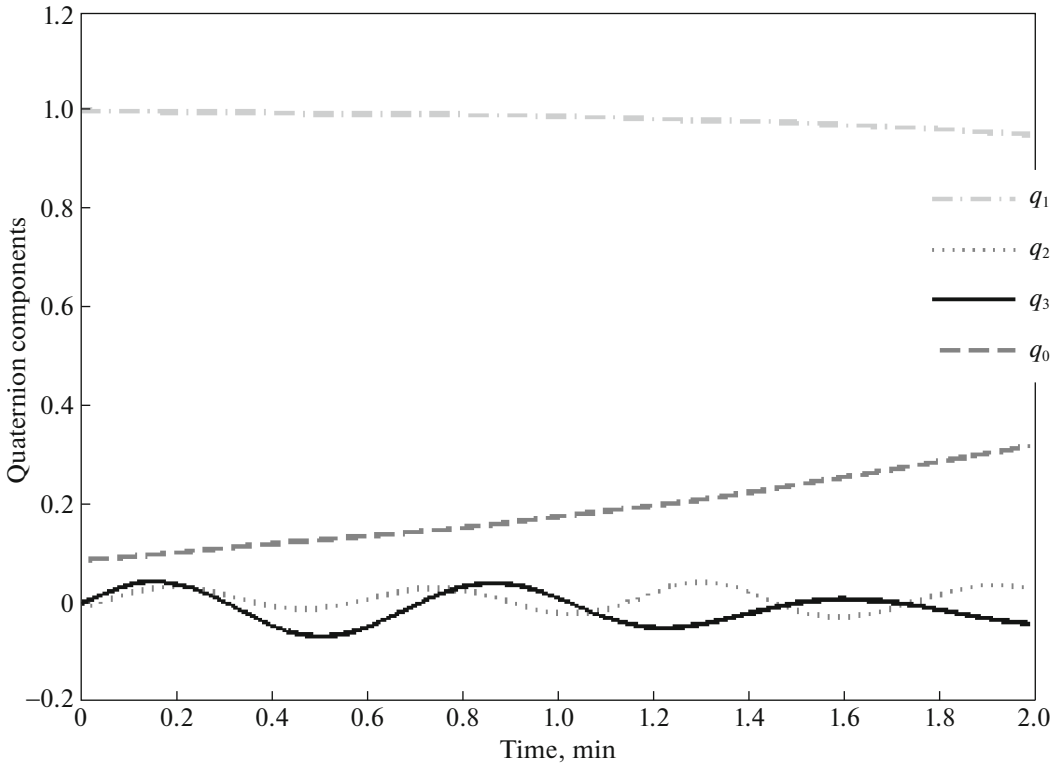

Fig. 10. Angular positions measured before the displacement of the loads.

mockup is shown in Fig. 11, while the estimated vector that describes the position of its center of mass is shown in Fig. 12. Then, upon convergence, the estimated position of the center of mass (in m) is

$$\mathbf{r} = \begin{bmatrix} -4.0\times10^{-6} \\ -1.0\times10^{-7} \\ -8.1\times10^{-5} \end{bmatrix}.$$

The error in the position of the center of mass estimated using the least squares method is 2×10^{-6} m.

Let us now consider the behavior of the estimates when moving the loads. Suppose that the loads are moved by the vector of [−10; −10; −50] mm, which corresponds to the displacement of the center of mass in terms of the above parameters by $[-1;-1;-5]\times10^{-5}$ m. Figure 13a shows an example where the information about the displacement of the loads is not included in the equations of motion for the Kalman filter. It can be seen that, beginning with approximately 120 s, the estimate tracks the current position of the center of mass with the variations in the corresponding vector being close to the computation: $[-1;-1;-5] \times 10^{-5}$ m. Figure 13b shows an example where the information about the displacement of the loads by the given value is included in the equations of motion for the Kalman filter. At the instant of 120 s, the estimates of the position of the center of mass are sharply shifted by $[-1;-1;-5]\times10^{-5}$ m; however, on the third component, this value gradually converges to 1.1×10^{-5} m, rather than to the computed value 1.4×10^{-5} m. This can be due to the fact that the computed displacement of the center of mass has certain error because of the inaccuracy of the linear actuators, execution error, or thermal expansion that causes the displacement of the center of mass.

Now, let us consider the combined operation of the algorithm for determining the center of mass and the automatic balancers. Suppose that the desired position of the center of mass is given by the vector $[0;0;-10] \times 10^{-5}$ m. In this case, the effect of the gravitational torque on the motion of the aerodynamic suspension can be reduced. Based on the estimated position of the center of mass found using the Kalman filter, every 25 s, the loads are shifted by the value that delivers the desired position of the center of mass.

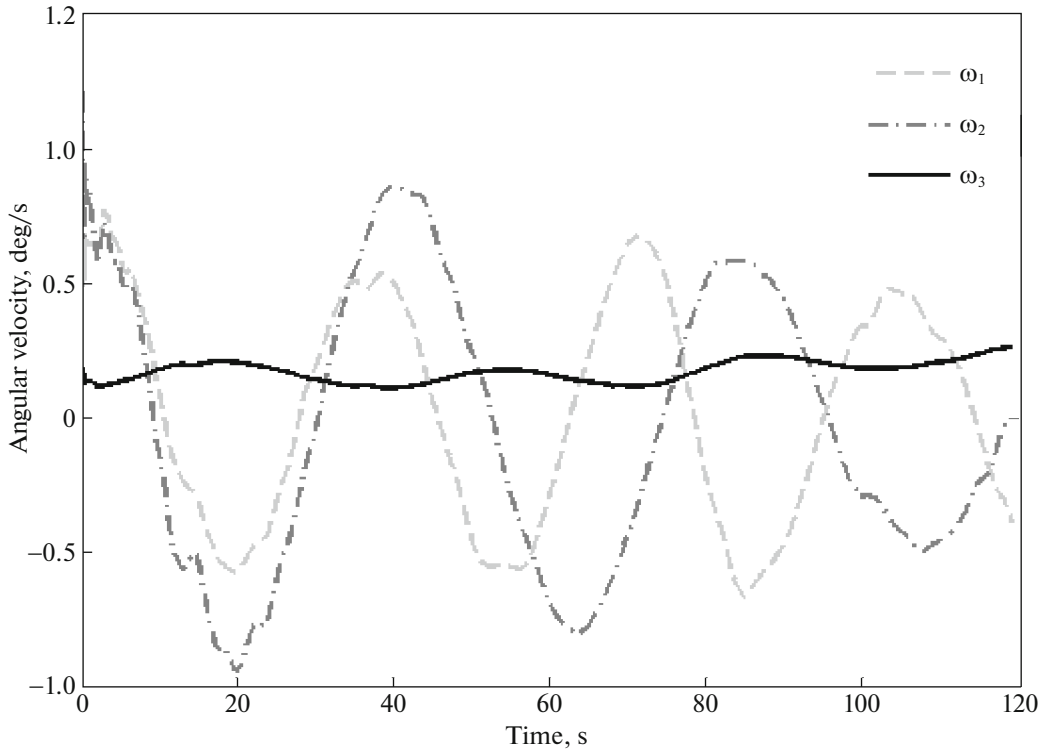

Fig. 11. Angular velocity estimates.

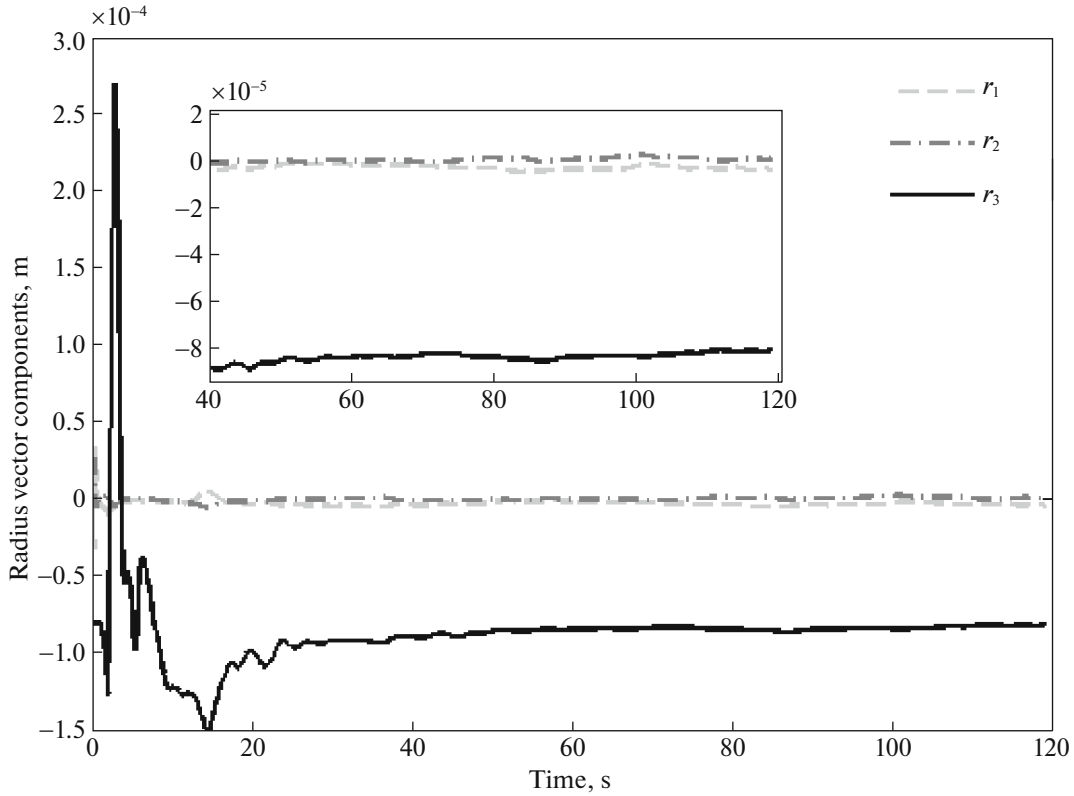

Fig. 12. Estimated components of the radius vector of the center of mass relative to the center of the suspension in the body-fixed frame of reference.

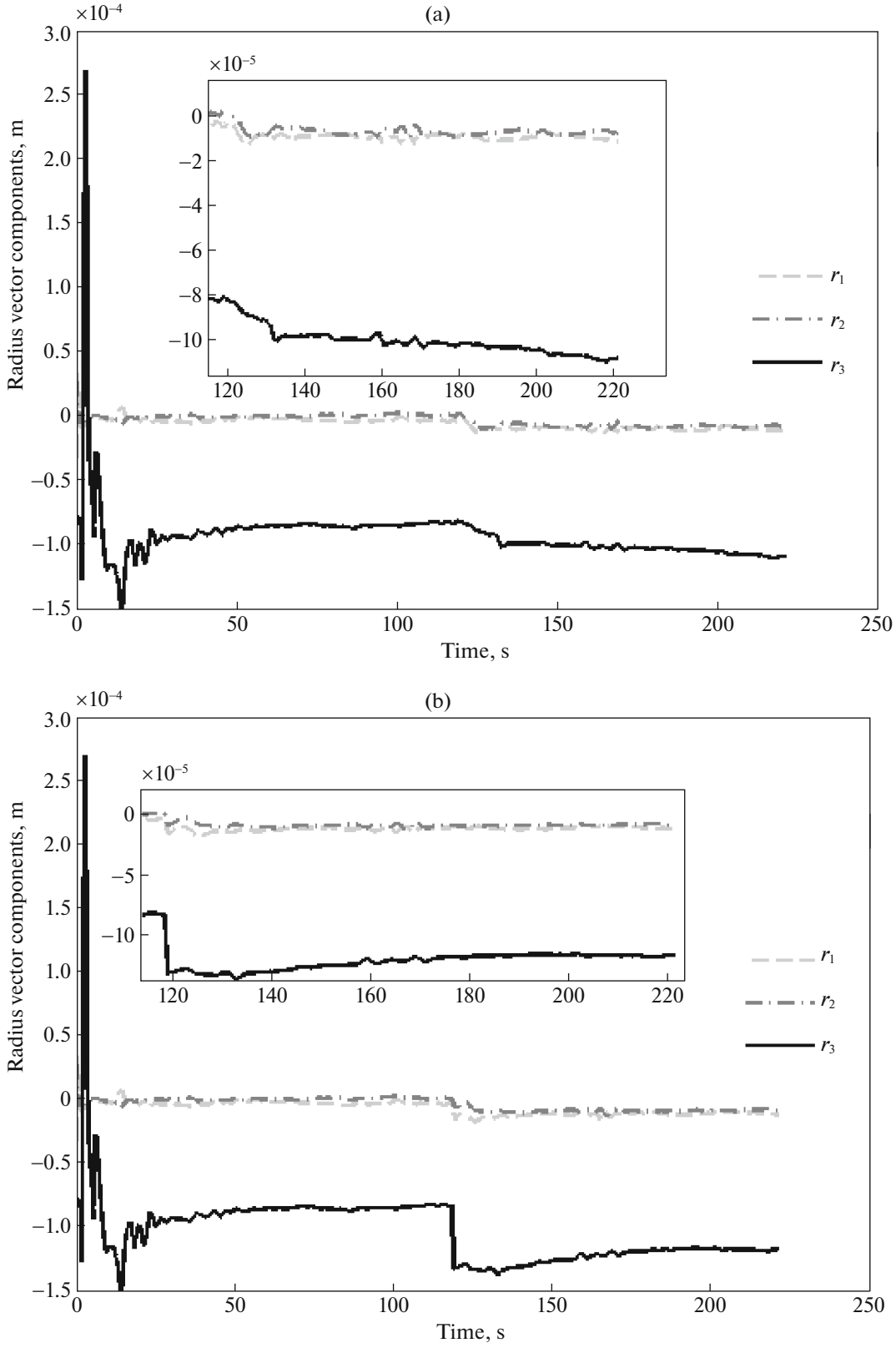

Fig. 13. Estimated components of the radius vector of the center of mass for the displaced loads when the information about the displacement is (a) included and (b) not included in the equations of motion for the Kalman filter.

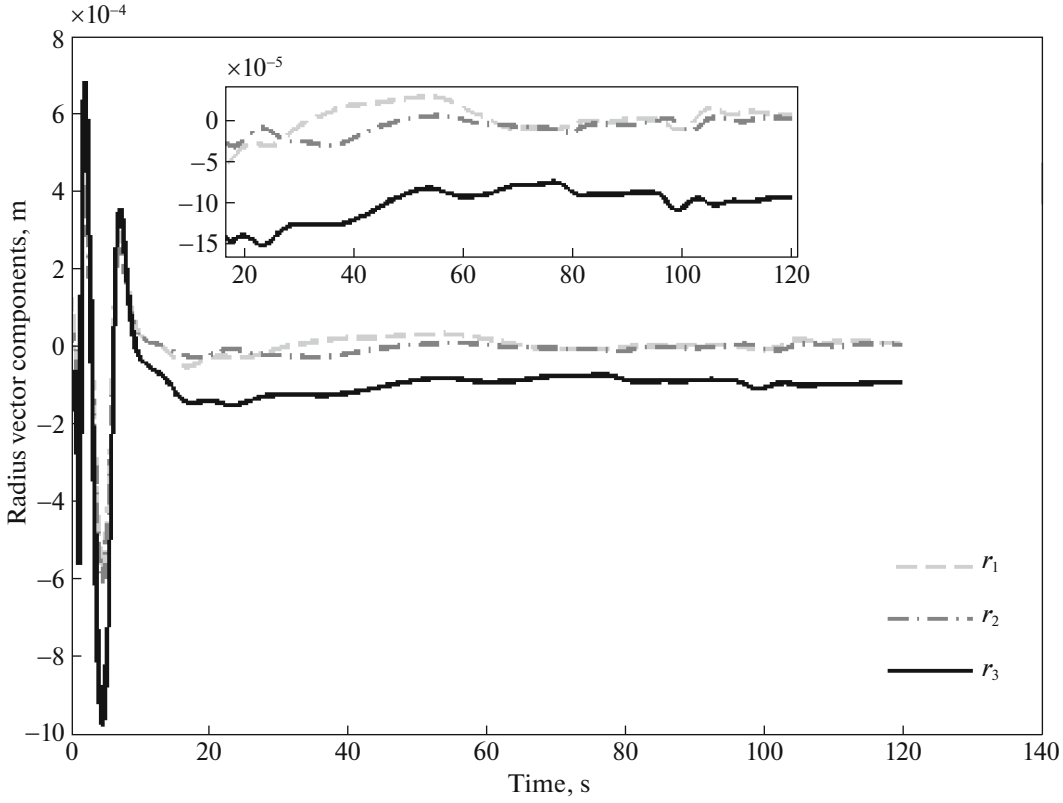

Fig. 14. Estimated position of the center of mass in the process of automatic balancing.

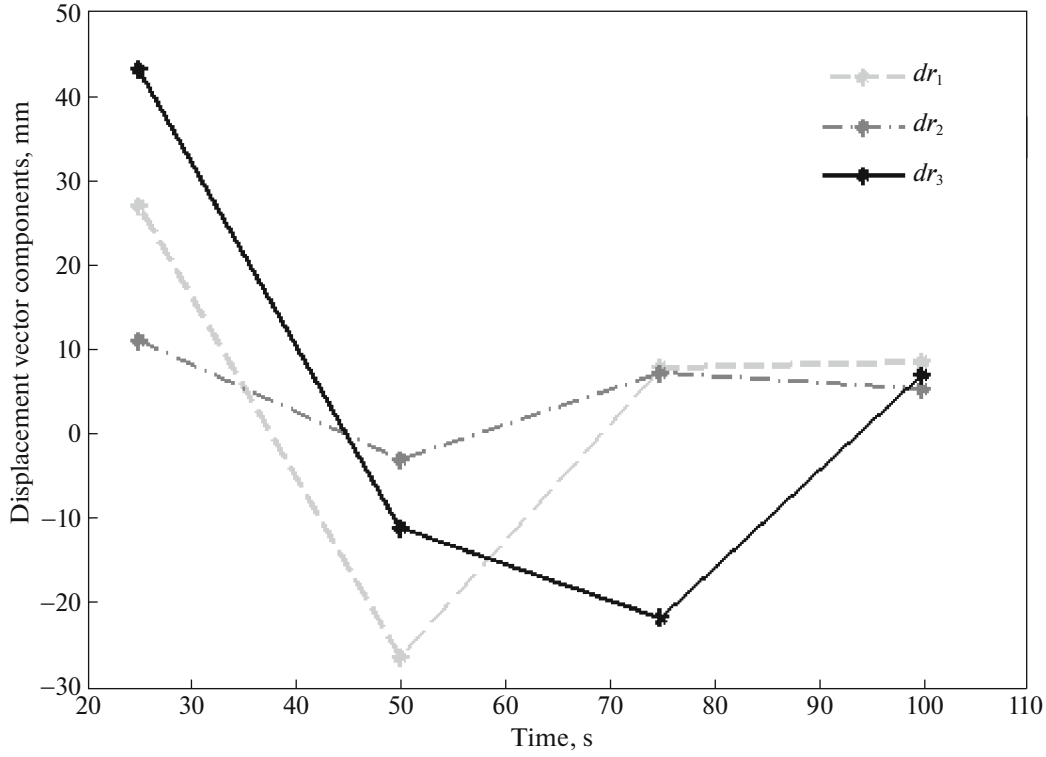

Fig. 15. Displacements of the loads in the process of automatic balancing.

However, due to errors in the estimated position of the center of mass, as well as thermal effects that cause its smooth displacement, the position of the center of mass needs to be gradually refined. Thus, due to the successive periodic displacements of the loads, the center of mass is set in a certain neighborhood of the desired position. Figure 14 shows the estimated positions of the center of mass found using the Kalman filter, while Fig. 15 shows the values of the balancing displacements computed based on the current positions of the center of mass every 25 s. As a result, after four iterations, the desired position of the center of mass is set accurate to about 1×10^{-5} m.

Thus, we have described the combined operation of the system for determining the position of the center of mass relative to the suspension point and the balancing system, which reduces the effect of the gravitational torque on the motion of the mockup on an aerodynamic suspension by shifting its center of mass closer to the center of the suspension.

CONCLUSIONS

When testing attitude control algorithms for satellites on ground-based testbeds with aerodynamic suspensions, it is required to reduce the effect of the disturbing gravitational torque on the motion of the attitude system mockup. In this paper, we have proposed a combination of algorithms for the two-stage balancing of a microsatellite mockup. At the first stage, the position of its center of mass relative to the center of rotation of the suspension, as well as the components of its inertia tensor, are estimated based on the known displacement of the balancing loads when the mockup is in free uncontrolled motion. This technique has been tested on the testbed designed by Sputnix with the accuracy of estimating the position of the center of mass being approximately 10 μm and the accuracy of estimating the diagonal elements of the inertia tensor being approximately 0.1 kg m^2. The estimate of the inertia tensor and the first approximation of the position of the center of mass have been used at the second stage of automatic balancing. In long-term experiments, thermal deformations cause the center of mass to shift. That is why its position has been estimated in real time by using the algorithm based on the Kalman filter and, based on this information, the loads were moved to set the center of mass to the desired position. During our experimental investigation of the developed technique on this testbed, we managed to ensure the desired position of the mockup's center of mass relative to the center of the suspension with an accuracy of approximately 10 μm, which is acceptable for testing onboard attitude control algorithms.

REFERENCES

1. D. S. Ivanov, M. D. Koptev, Ya. V. Mashtakov, M. Yu. Ovchinnikov, N. N. Proshunin, S. S. Tkachev, A. I. Fedoseev, and M. O. Shachkov, "Laboratory facility for microsatellite mock-up motion simulation," J. Comput. Syst. Sci. Int. **57**, 115 (2018).
2. D. Ivanov, M. Koptev, Y. Mashtakov, et al., "Determination of disturbances acting on small satellite mock-up on air bearing table," Acta Astronaut. **142**, 265–276 (2018).
3. D. Bindel', I. E. Zaramenskikh, D. S. Ivanov, M. Yu. Ovchinnikov, and N. G. Proncheva, "A laboratory facility for verification of control algorithms for a group of satellites," J. Comput. Syst. Sci. Int. **48**, 779 (2009).
4. M. Ovchinnikov, D. Ivanov, N. Ivlev, et al., "Development, integrated investigation, laboratory and in-flight testing of Chibis-M microsatellite ADCS," Acta Astronaut. **93**, 23–33 (2014).
5. D. S. Ivanov, S. O. Karpenko, M. Yu. Ovchinnikov, D. S. Roldugin, and S. S. Tkachev, "Testing of attitude control algorithms for microsatellite Chibis-M at laboratory facility," J. Comput. Syst. Sci. Int. **51**, 106 (2012).
6. W. Haeussermann and H. Kennel, "A satellite motion simulator," Automatica **5** (12), 22–25, 90–91 (1960).
7. M. Peck, L. Miller, A. Cavender, et al., "An airbearing-based testbed for momentum control systems and spacecraft line of sight," Adv. Astronaut. Sci. **114**, AAS 03–127 (2003).
8. D. Ivanov, M. Koptev, M. Ovchinnikov, et al., "Flexible microsatellite mock-up docking with non-cooperative target on planar air bearing test bed," Acta Astronaut. **153**, 357–366 (2018).
9. S. S. F. Cordova and D. B. DeBra, "Mass center estimation of a drag-free satellite," in *Proceedings of the 6th Triennial World Congress of the IFAC, Boston, 1975.*
10. J. Prado, G. Bisiacchi, L. Reyes, et al., "Three-axis air-bearing based platform for small satellite attitude determination and control simulation," J. Appl. Res. Technol. **3**, 222–237 (2005).
11. M. A. Post, J. Li, and R. Lee, "Design and construction of a magnetic field simulator for CubeSat attitude control testing," J. Instrum. Autom. Syst. **1** (1), 1–9 (2014).
12. M. Pastena, L. Sorrentino, and M. Grassi, "Design and validation of the university of Naples space magnetic field simulator (SMAFIS)," J. Inst. Environ. Sci. Technol. **44**, 33–42 (2001).

13. M. Prinkey, D. Miller, P. Bauer, et al., "CubeSat attitude control testbed design: Merritt 4–Coil per axis Helmholtz cage and spherical air bearing," in *Proceedings of the AIAA Guidance, Navigation, and Control (GNC) Conference, Reston, Virginia, 2013.*
14. R. Silva, I. Ishioka, C. Cappelletti, et al., "Helmholtz cage design and validation for nanosatellites HWIL testing," IEEE Trans. Aerospace Electron. Syst. **55**, 3050–3061 (2019).
15. M. Romano and B. N. Agrawal, "Acquisition, tracking and pointing control of the bifocal relay mirror spacecraft," Acta Astronaut. **53**, 509–519 (2003).
16. J. J. Kim and B. N. Agrawal, "Automatic mass balancing of air-bearing-based three-axis rotational spacecraft simulator," J. Guidance, Control, Dyn. **32**, 1005–1017 (2009).
17. S. Wang, J. Ma, and S. Gao, "Balancing methods on the three-axis air-bearing platform," in *Proceedings of the Asia Simulation Conference, Shaghai* (Springer, 2012), pp. 117–125.
18. S. Chesi, Q. Gong, V. Pellegrini, et al., "Automatic mass balancing of a spacecraft three-axis simulator: analysis and experimentation," J. Guidance, Control, Dyn. **37**, 197–206 (2014).
19. Z. Xu, N. Qi, and Y. Chen, "Parameter estimation of a three-axis spacecraft simulator using recursive least-squares approach with tracking differentiator and extended Kalman filter," Acta Astronaut. **117**, 254–262 (2015).
20. A. Krishnanunni, S. Jayadevan, A. Mony, et al., "Inertia and center of mass estimation of a 3 DoF air bearing platform," IFAC-PapersOnLine **51**, 219–224 (2018).
21. Z. Xu, Y. Chen, and Z. Xu, "A suboptimal excitation torque for parameter estimation of a 5–DOF spacecraft simulator," Adv. Space Res. **62**, 2556–2565 (2018).
22. SPUTNIKS–Test Benches. https://sputnix.ru/ru/oborudovanie/ispytatelnye-stendy/. Accessed February12, 2020.
23. V. N. Branets, *Lectures on the Theory of Strapdown Inertial Navigation Control Systems* (MFTI, Moscow, 2009) [in Russian].
24. R. E. Kalman, "A new approach to linear filtering and prediction problems," Trans. ASME, Ser. D: J. Basic Eng. **82**, 35–45 (1960).
25. M. Ovchinnikov and D. Ivanov, "Approach to study satellite attitude determination algorithms," Acta Astronaut. **98**, 133–137 (2014).

Translated by Yu. Kornienko